

On the Structure Selectivity of Mixed Gas Hydrates and Group 14 Clathrates

Masakazu Matsumoto¹ and Hideki Tanaka²

¹Research Institute for Interdisciplinary Science, Okayama University, Okayama 700-8530, Japan; orcid.org/0000-0002-6799-6813; Email: vitroid@gmail.com

²Toyota Physical and Chemical Research Institute, Aichi 480-1192, Japan; orcid.org/0000-0003-2099-8990;

The structure selectivity of mixed gas hydrates and group 14 clathrates is examined based on statistical mechanical theories and the empirical rule on the topological constraint of the Frank-Kasper phases. The most stable structure is revealed by the generalized phase diagram where the chemical potential differences in the three canonical forms of clathrates are independent variables. The most stable structure incorporating individual guest species is evaluated by the locus of the chemical potential differences on this generalized phase diagram. We show that the method developed here is simple but powerful to estimate roughly phase behaviors of clathrate compounds in a wide range of thermodynamic conditions, which is demonstrated by two applications, the generalized phase diagram of group 14 element clathrates and the phase behavior of mixed gas hydrates. The present theory leads to proposals of phase change agents, addition of which sensitively influences the structure selectivity, encompassing even minor structures.

Introduction

Clathrate hydrates are solid solutions of water and small guest molecules. Among them, methane hydrate is widely distributed in permafrost and ocean floor and is attracting attention not only as an energy resource but also as a source of greenhouse gases that have a significant impact on climate change.^{1,2} For pure guest molecules, there are two major crystal structures, type I (sI, cubic structure I, CS-I) and type II (sII, cubic structure II, CS-II).³ An exception is Br₂ hydrate, which is known to have a type III (sIII, tetragonal structure, TS-I) crystal structure.^{4,5} Empirically, the crystal structures are determined by the size of the guest molecules.⁶ A guest molecule is captured inside a cage composed of water molecules. The cage consists only of five- and six-membered rings formed by hydrogen bonds in these structures.

The family of crystalline structures with empty cages made of only five- and six-membered rings is called Frank–Kasper (FK) clathrates (a.k.a. space-fullerenes).⁷ It has shown that there are a wide variety of structures in the FK clathrate family. However, the only FK clathrate hydrate structures ever found in nature are type I, II, or III. A similar phenomenon has been observed in clathrate compounds of group 14 elements, which also form type I or II in most cases and rarely type III.^{8,9}

An attempt to elucidate the crystal structure selection rule for clathrate hydrates was made by Matsumoto et al.¹⁰ They combined the topological constraints on the crystal structure of FK clathrate hydrates¹¹ with the standard theory of stability of clathrate hydrates,¹² and found that the stability of the crystals is governed by a small number of parameters. This revealed that no matter how sophisticatedly one adjusts the temperature, guest molecular species, or their partial pressures, only a few FK clathrates out of many candidates can be the most stable phase in a wide range of thermodynamic conditions. Furthermore, the reason why bromine exceptionally produces type III crystals was elucidated. The variety of the possible stable phases is visualized by the generalized phase diagram (GPD).¹³

In this paper, we review their theory and discuss how the phase boundaries of GPD are settled. The selection rule based on the stability theory with the empirical constraints is simple but quite useful. We show its applicability by examining GPD for the FK clathrate compounds of group 14 elements. In another application, we discuss why a small variation in

the composition and the interaction potential of the guest molecules gives rise to structural transition and thus exhibits a rich variety of crystal structures. Finally, we discuss how to design gas mixtures to generate crystal structures that would not occur in equilibrium with a single guest species.

In our previous studies, we have made various improvements to the vdWP theory, aiming to predict the physical properties more accurately by removing the assumptions on which the theory was based.^{14–17} In this study, conversely, we aim to shed light on the mathematical structure behind the theory and derive general regularities by introducing an additional assumption to the vdWP theory.

Method

The original vdWP theory

The van der Waals–Platteeuw (vdWP) theory, the standard theory for clathrate hydrates, introduces three assumptions:

1. The occupation of a guest molecule in a given cage is independent of the other cages.
2. Guest molecules do not affect the vibrations of the host lattice.
3. Each cage contains at most one guest molecule.

Under these assumptions, the chemical potential μ_c of water molecules in clathrate hydrates can be divided into a term μ_c^0 on the host lattice, which consists only of water molecules, and a term $\Delta\mu_c$ on guest molecules, which are incorporated into cages in the host lattice.

$$\mu_c = \mu_c^0 + \Delta\mu_c. \quad (1)$$

If the guest molecule is a single component, the guest term can be written as follows:

$$\Delta\mu_c = \sum_k \alpha_k \Delta\mu_e^{(k)}, \quad (2)$$

$$\Delta\mu_e^{(k)} = -k_B T \ln \left(1 + \exp \left[\beta \left(\mu_g - f_g^{(k)} \right) \right] \right), \quad (3)$$

where $\alpha_k = N_k/N_W$ is the number of k -hedral cages relative to the number of water molecules N_W , μ_g is the chemical potential of the guest molecules, $f_g^{(k)}$ is the free energy of cage occupation in the k -hedral cage, and $\beta = 1/k_B T$. This corresponds to considering the equilibrium between clathrate hydrate and pure guest species without referring to the equilibrium between clathrate hydrate and water.¹⁶

The extended theory

In addition to these three assumptions, Matsumoto et al. introduced a fourth assumption that the occupation free energy $f_g^{(k)}$ of a k -hedral cage is common across any crystal structure.¹⁰

The FK clathrate is a clathrate in which all cages are one of 12-, 14-, 15-, and 16-hedra consisting only of pentagonal and hexagonal faces.¹⁸ The name FK phase is known as a category of alloy structures; all atoms are either 12-, 14-, 15-, or 16-coordinated in FK alloys. It also belongs to a type of topologically close-packed structure (TCP) in which adjacent atoms are always packed tetrahedrally. An FK alloy structure and the corresponding FK clathrate structure are dual; Voronoi cells of FK alloy form the FK clathrate structure. The preference of water molecules to be four-coordinated is the cause of the FK type clathrate structure.¹⁹ There are several clathrate hydrate crystal structures that are not FK-type: e.g. type H (HS-III), filled ice (C_0 , C_1 , and C_2 phases)²⁰⁻²², and other high-pressure phases, where large distortions of the hydrogen bonds are allowed.

The Yarmolyuk-Kripyakevich (YK) empirical rule is a topological constraint on the coordination number. It asserts that the composition ratios of 12-, 14-, 15-, and 16-coordinated atoms in any FK alloy can be represented by a linear combination of the composition ratios of 12-, 14-, 15-, and 16-coordinated atoms in the three canonical FK alloy structures, A15, C15 and Z. This rule is also valid for the FK clathrates due to the duality; the composition ratios of the 12-, 14-, 15-, and 16-hedral cages of any FK clathrate can be expressed as a linear combination of the number of cages in the three canonical FK clathrate structures, sI (CS-I), sII (CS-II), and sIV (HS-I). Matsumoto et al. took account of the number of water molecules constituting each cage and derived the constraints imposed on the crystal structure of FK clathrate as follows:¹⁰ According to the YK rule, the number of k -hedral cages ($k=12,14,15$, or 16) for a given crystal structure A can be expressed as a linear sum of three canonical crystal structures, namely

$$\alpha_k^{(A)} = x_A \alpha_k^{(\text{CS I})} + y_A \alpha_k^{(\text{CS II})} + z_A \alpha_k^{(\text{HS I})}. \quad (4)$$

Or, with a matrix and vectors,

$$(\alpha_{12}^{(A)}, \alpha_{14}^{(A)}, \alpha_{15}^{(A)}, \alpha_{16}^{(A)}) = (x_A, y_A, z_A) \begin{pmatrix} \alpha_{12}^{(\text{CS-I})} & \alpha_{14}^{(\text{CS-I})} & \alpha_{15}^{(\text{CS-I})} & \alpha_{16}^{(\text{CS-I})} \\ \alpha_{12}^{(\text{CS-II})} & \alpha_{14}^{(\text{CS-II})} & \alpha_{15}^{(\text{CS-II})} & \alpha_{16}^{(\text{CS-II})} \\ \alpha_{12}^{(\text{HS-I})} & \alpha_{14}^{(\text{HS-I})} & \alpha_{15}^{(\text{HS-I})} & \alpha_{16}^{(\text{HS-I})} \end{pmatrix}, \quad (5)$$

where (x_A, y_A, z_A) is the composition ratio unique to the structure A and satisfies $x + y + z = 1$. For example, the composition ratios for sI (CS-I), sII (CS-II), sIII (TS-I), and sIV (HS-I) are $(x, y, z) = (1,0,0), (0,1,0), (23/43,0,20/43), (0,0,1)$, respectively.¹⁰

As shown in Equation 2, the guest term $\Delta\mu_c$ can be written in the form of a linear combination of $\Delta\mu_e^{(k)}$ with $\alpha_k^{(A)}$ as the coefficient and it is allowed by the fourth assumption to use common $\Delta\mu_e^{(k)}$ for any crystal structures having k -hedral cages. Once the guest term $\Delta\mu_c$ is calculated for three canonical crystal structures, the guest terms $\Delta\mu_c$ for any other crystal structure can be given by linear combination with the composition ratio as the coefficient.

$$\Delta\mu_c^{(A)} = x_A \Delta\mu_c^{(\text{CS I})} + y_A \Delta\mu_c^{(\text{CS II})} + z_A \Delta\mu_c^{(\text{HS I})}. \quad (6)$$

The host term μ_c^0 is not affected by the guest due to the second assumption of the vdWP theory and is determined immediately when the crystal structure is chosen. Thus, the only externally manipulable variable is the guest term $\Delta\mu_c$ for three canonical crystal structures. Their relative magnitudes can be varied by the molecular species and partial pressures of the guest molecules, but no matter how they are varied, the crystal structure selectivity is governed only through the guest term, $\Delta\mu_c$.

The generalized phase diagram

As mentioned above, the guest term $\Delta\mu_c$ of the chemical potential of a typical FK clathrate hydrate is readily evaluated by the guest terms $\Delta\mu_c$ of three canonical structures. Thus, we can find which of these crystal structures is the most stable. It is natural to draw the phase diagram against the guest term $\Delta\mu_c$ of the three canonical crystal structures. Matsumoto et al. proposed a GPD choosing the guest terms $\Delta\mu_c$ of the three canonical structures as free variables.¹³ The GPD for FK clathrate hydrates are shown in Figure 1. In this plot, they selected $X = \Delta\mu_c^{(\text{CS I})} - \Delta\mu_c^{(\text{HS I})}$ for the horizontal axis and $Y = \Delta\mu_c^{(\text{CS II})} - \Delta\mu_c^{(\text{HS I})}$ for the

vertical axis.¹⁰ The present paper follows this drawing convention. The GPD makes it possible to infer in advance which crystal structure can be the most stable or second most stable phase from only the information of the host lattice without designating the guest species or partial pressures as shown below.

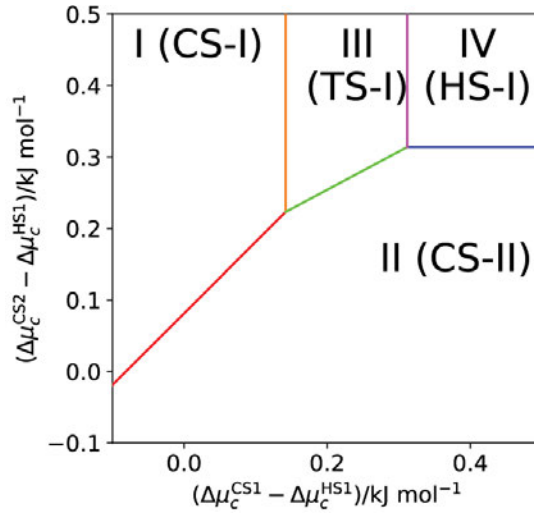


Figure 1. GPD of FK clathrate hydrates. TIP4P/ICE water model, 273 K, 5 MPa.

Geometry of Coexistence Lines

We explain how the position and slope of the coexistence line on GPD of clathrate hydrate are determined. Let us find the coexistence line of two FK clathrate structures, say A and B. The chemical potential of water molecules in crystal A can be expressed by a host term $\mu_c^{0(A)}$, which is dependent only on the host lattice structure, and a guest term $\Delta\mu_c^{(A)}$, which is derived from the interaction and partial pressure of guest molecules. The latter can further be expressed as a linear sum of the three canonical structures.

$$\mu_c^{(A)} = \mu_c^{0(A)} + \Delta\mu_c^{(A)} = \mu_c^{0(A)} + x_A\Delta\mu_c^{(CS\ I)} + y_A\Delta\mu_c^{(CS\ II)} + z_A\Delta\mu_c^{(HS\ I)}, \quad (7)$$

where x_A, y_A, z_A are the composition ratios of structure A. The same is valid for B. On the coexistence, $\mu_c^{(A)} = \mu_c^{(B)}$, therefore,

$$\mu_c^{0(A)} + x_A\Delta\mu_c^{(CS\ I)} + y_A\Delta\mu_c^{(CS\ II)} + z_A\Delta\mu_c^{(HS\ I)} = \mu_c^{0(B)} + x_B\Delta\mu_c^{(CS\ I)} + y_B\Delta\mu_c^{(CS\ II)} + z_B\Delta\mu_c^{(HS\ I)}. \quad (8)$$

Organizing the equation by introducing the constraint on the composition ratio $x_A + y_A + z_A = 1$ and we finally have an equation for a straight line.

$$(x_A - x_B)X + (y_A - y_B)Y + \left(\mu_c^{0(A)} - \mu_c^{0(B)}\right) = 0. \quad (9)$$

It indicates that the slope is determined by the composition ratios of two phases and the intercept is determined by the difference in the host terms of two structures.

For example, the coexistence line between type I and II, drawn with a red line in Figure 1, is obtained by introducing their component ratios, $(x, y, z)_{CS\ I} = (1,0,0)$ and $(x, y, z)_{CS\ II} = (0,1,0)$, to the equation:

$$Y = X + \left(\mu_c^{0(CS\ I)} - \mu_c^{0(CS\ II)}\right). \quad (10)$$

Its slope is unity and intercept is the difference in the host term between two structures, which is typically positive.

Similarly, the coexistence line between type II (CS-II) and type IV (HS-I, $(x, y, z)_{HS\ I} = (0,0,1)$), drawn with a blue line in Figure 1, is obtained as

$$Y = \mu_c^{0(HS\ I)} - \mu_c^{0(CS\ II)}. \quad (11)$$

Its slope is zero and intercept is the difference in the host term between two structures, which is typically positive.

The coexistence line between type I and IV is obtained in the same way as

$$X = \mu_c^{0(HS\ I)} - \mu_c^{0(CS\ I)}. \quad (12)$$

The right hand side is typically positive. Note that this is a metastable coexistence line that does not appear in Figure 1 because type III (TS-1) intervenes I and IV.

Thus, all coexistence lines are linear, all slopes are determined by the composition ratios, and all intercepts are determined by the host terms, μ_c^0 on GPD. No guest information is necessary to draw the diagram, and therefore it is computationally very inexpensive.

Applications

Generalized phase diagram of group 14 element clathrates

The vdWP theory can be applied not only to clathrate hydrates but also to clathrate compounds such as silicon and silica, which have the same geometric structure. In the case of group 14 inorganic clathrate compounds such as silicon, the types of crystal structures actually formed are limited to few, mostly type I or type II although the crystal structure is allowed to change depending on the guest atoms contained (typically alkali metal elements such as Na and Li) as well as temperature and pressure.⁸ Compared to the more than 200 known crystal structures of zeolite, i.e., allotrope of silica, there is very little diversity in the crystal structures of group 14 clathrate alloys. The reason has been guessed that the bonds that make up the network of silicon are not as flexible as Si-O-Si bonds.⁸ Type III clathrate was identified in Sn in 2001,⁹ but it is considered to be a “line compound”, existing only in a very narrow composition ratio.⁵ Other than those FK clathrates, several non-FK clathrates have also been found.^{23–27}

Karttunen et al. reported the potential energy E_p^0 of the host lattice of the group 14 element clathrates by quantum-chemical calculations.²⁸ At low temperatures, the free energy can be approximated by the potential energy, so replacing the host term μ_c^0 with E_p^0 allows GPD to be drawn with known information, as shown in Figure 2. Among the structures treated by Karttunen et al., we adopt the following structure, which belongs to the FK crystal family: I (A15, CS-I), II (C15, CS-II), III (σ , TS-I), IV (Z, HS-I), V (C14, HS-II), II+4H (C36), II+IV-a (T), II+IV-b (μ), where the nomenclature of the corresponding alloy structures is also listed in parentheses.

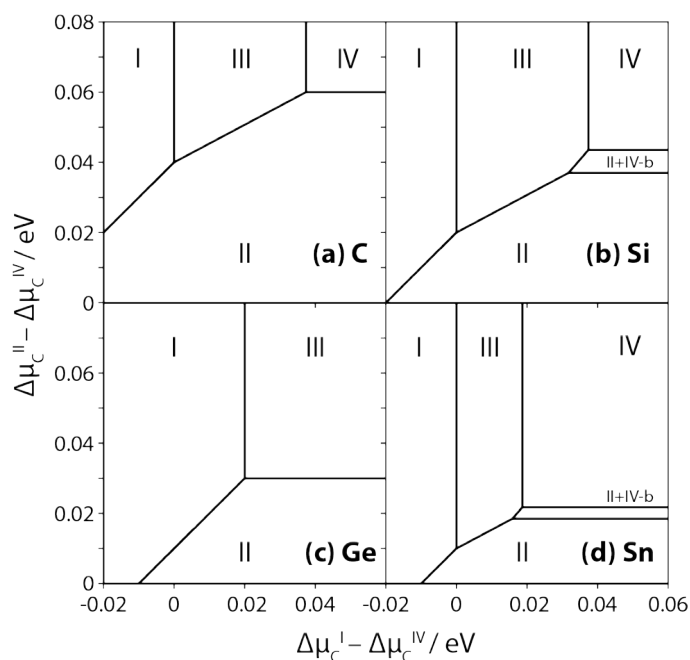


Figure 2. Generalized phase diagrams of the group 14 element clathrates based on the first-principle calculations by Karttunen et al. (a) C, (b) Si, (c) Ge, (d) Sn. Of the structures calculated by Karttunen et al., eight FK-type crystals are evaluated.

Even if the element constituting the crystal is changed from a water molecule to a group 14 element, the apparent feature of the GPD looks alike, and it is predicted that only the limited types of the crystal structure can form among many FK clathrate structures. That is, structures I, II, III, IV, and rarely II+IV-b may be more stable than others. In reality, no clathrate structure has been made with carbon, but if it can, it is expected to be a superhard material.²⁹ Silicon clathrate is expected to improve the performance of solar cells.³⁰

The use of the GPD is advantageous because it does not require information on guests to predict the possible stable phases.

Phase behavior of mixed gas hydrates

The GPD provides a complete picture of the possible crystal structures. For example, it is predicted from the GPD that the FK clathrate hydrate cannot be thermodynamically most stable except for four types CS-I, CS-II, HS-I, and TS-I, as shown in Figure 1, and the second most stable phases are also limited.^{10,13} The hydrate states of various real gases can also be

conducted as shown in Figure 3. For example, the state of methane hydrate under certain thermodynamic conditions is indicated on the GPD by a state point $(X, Y) = (\Delta\mu_c^{(\text{CS I})} - \Delta\mu_c^{(\text{HS I})}, \Delta\mu_c^{(\text{CS II})} - \Delta\mu_c^{(\text{HS I})})$, where $\Delta\mu_c^{(A)}$ represents the guest term of the chemical potential of the water molecule when the methane hydrate is a crystal structure A. If this point falls into the region I on the diagram, it indicates that methane hydrate will become type I structure under the given condition.

The positions of the coexistence lines on the GPD hardly vary with temperature and pressure. This is because temperature and pressure do not stabilize preferentially a specific canonical structure and because the gradient of the coexistence line depends only on the composition ratio. For very small guest molecules, multiple occupancy of the cage may be taken into consideration by exact or approximate method in the framework of the vdWP theory.^{14,31} However, since multiple occupancy does not affect the linearity of the chemical potential of water in Eq. (3), it does not affect the coexistence lines in the GPD, but only shifts the loci of the individual molecules.

It is known that crystal structure in equilibrium with a binary gas mixture may be transformed with varying composition. For example, both methane and ethane form type I hydrate, whereas methane-ethane double hydrates change to type II depending on the mixing ratio.^{32,33} Similar phenomena have been observed in methane-cyclopropane double clathrate hydrates.³⁴ On the contrary, mixing of methane and ethylene does not change the structure although the molecular size of ethylene is close to that of ethane.³⁵ Let us take a close look at these tendencies on the GPD.

Mixing of gases replaces the guest term in eq. 3 with the following form.

$$\Delta\mu_e^{(k)} = -k_B T \ln \left(1 + \sum_j \exp \left[\beta (\mu_j - f_j^{(k)}) \right] \right), \quad (13)$$

where μ_j is the chemical potential of the guest component j , and $f_j^{(k)}$ is the free energy of the cage occupation by guest component j incorporated in the k -hedral cage. In the following, μ_j is calculated assuming that the guest molecule is an ideal gas. The temperature is fixed at 273.15 K and the total pressure is fixed at 50 bar unless otherwise stated but each partial pressure of the binary mixture is varied. To simplify, the guest molecules are approximated

by a single point Lennard-Jones particle, the parameters of which are shown in Table 1. We employ a hypothetical bromine-like molecule, say Q, which forms type III hydrate at 10 bar according to our estimation. The TIP4P/Ice model is employed for water molecules,³⁶ and the water-guest interaction is estimated based on the Lorentz–Berthelot rule.

Table 1. The Lennard-Jones parameters of the guest molecules and their hydrate structures.

	σ (Å)	ϵ/k_B (K)	Struc.	Ref.
Ne	2.749	35.6	II	c
Ar	3.405	119.8	II	c
Kr	3.60	171.0	II	c
Methane	3.758	148.6	I	a
Xe	4.047	231.0	I	a
Ethylene	4.232	205	I	c
CS ₂	4.438	488	I	c
CO ₂	4.486	189.0	I	a
Ethane	4.520	208.8	I	b
cyclopropane	4.582	301.5	II [†] , I ³⁷	e
Q	4.93	540	III [‡] , I	d
n-Butane	4.997	410	II	c

[†] at 0.75 bar, [‡] at 10 bar, a: Ref.³⁸, b: Ref.³³, c: Ref.³⁹, d: Ref.¹⁰, e: Estimated from the critical temperature and pressure.⁴⁰

One hundred different hydrogen-bond arrangements are generated for each empty clathrate hydrates of CS-I, CS-II, TS-I, and HS-I structures using the GenIce tool⁴¹ and the structures are optimized under constant pressure to estimate the density and the host term of the chemical potential of water, μ_c^0 . The latter is evaluated by quasi harmonic approximation with classical mechanical free energy.⁴² These thermodynamic properties are listed in Table 2. The

Lennard-Jones-Devonshire spherical approximation is used for calculating the free energy of the cage occupation, $f_j^{(k)}$,⁴³ in which the guest molecule interacts with the corresponding cage only. More advanced treatment of the interactions with the host lattice and other guests is discussed elsewhere,¹⁵ but we do not seek the accuracy here. In the calculation, entropic terms arising from the hydrogen disordering are negligible by the cancellation. The radius of each type of cage is shown in Table 3. The values can be compared with the experimental measurements.⁴⁴⁻⁴⁶

Table 2. The thermodynamic properties of the empty clathrate hydrate structures at 273.15 K, 5 MPa.

	$\mu_c^0 / \text{kJ mol}^{-1}$	$\rho / \text{g cm}^{-3}$
CS-I	-59.841	0.7921
CS-II	-59.923	0.7813
TS-I	-59.775	0.7899
HS-I	-59.609	0.7886

Table 3. The approximated radii of cages.

	$R / \text{\AA}$
12-hedron	3.988
14-hedron	4.331
15-hedron	4.527
16-hedron	4.587

The loci of the state points of single-component gas hydrates are plotted as a function of pressure in Figure 3(a). The points on the GPD move linearly with a common slope, $-\frac{23}{17}$, but the displacements by pressure are different for each molecular species. The derivation of the slope is discussed in Appendix. They move considerably in the case of relatively large guest

molecules. The cyclopropane hydrate changes to type II only when the pressure is very low, as is expected.³⁷

The loci of the state point on the GPD corresponding to the change of composition of the binary gas mixture are shown in Figure 3(b). The locus of the methane-ethane hydrate shows a loop indicating that it becomes type II when ethane is dilute. On the other hand, no loop emerges when methane is mixed with ethylene. It is easily predictable from the general tendencies in Figure 3 that if two guest species that both form sI by themselves yield sII by mixing at some compositions, the composition range would be narrower at higher pressures because the loop moves upward to the left. The prediction is consistent with the previous studies.^{47,48}

A particularly large loop appears when Q is mixed with a typical guest species forming type I structure. Q itself forms type I hydrate at 50 bar. A very small amount of Q mixed with any sort of guest changes the crystal structure to type II, and the loci of the state points also go through the region of type III. Consequently, mixing of these gases yields three different structures.

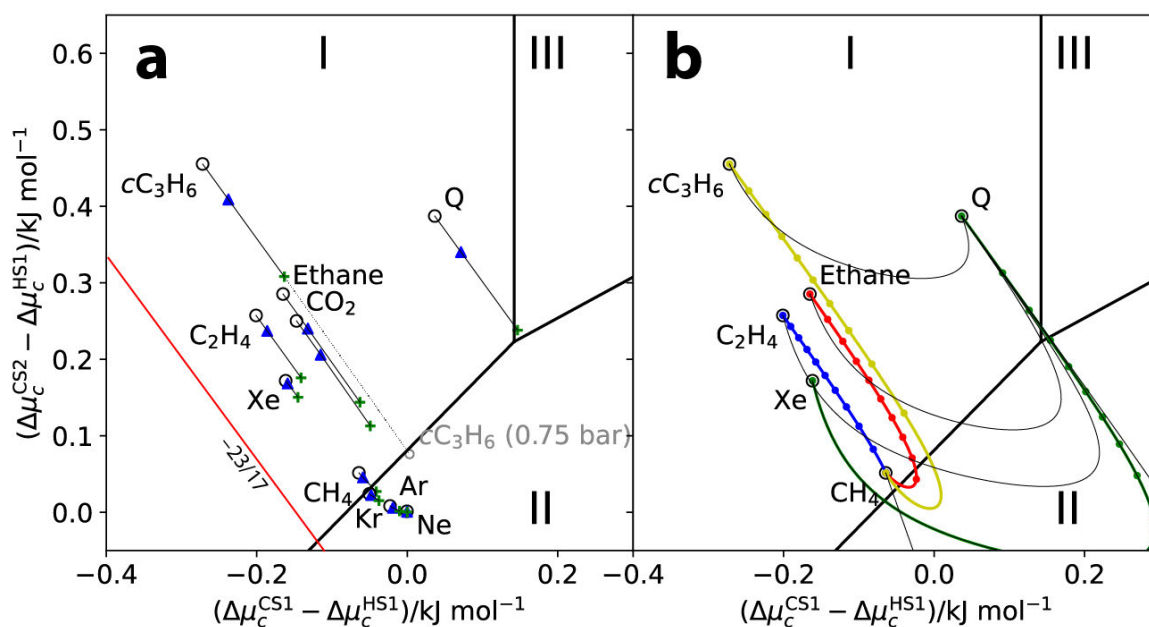


Figure 3. (a) Loci of $(X, Y) = (\Delta\mu_c^{(CS\ I)} - \Delta\mu_c^{(HS\ I)}, \Delta\mu_c^{(CS\ II)} - \Delta\mu_c^{(HS\ I)})$ on the GPD with

decreasing the pressure. Open circle, triangle, and cross symbols indicate the phases of the single-component gas hydrate at 50, 30, and 10 bar, respectively. The red line indicates the slope of $-23/17$. (b) Loci with the change of composition for mixtures of binary guest species. Total pressure of gases is fixed to 50 bar. Red, blue, green, and yellow curves indicate the loci of mixing (methane and ethane), (methane and ethylene), (xenon and Q), and (methane and cyclopropane), respectively. Dots were drawn for every 10% increase in mole fraction. The thin lines represent the loci of various guests mixed with Q.

Thus, Q could work as a generic *phase change agent*. Any typical guest species forming type I structure is expected to change to type II with a small amount of Q, as shown in Figure 4 (a).

We may ask which guest species is capable of exerting the most abundant structural diversity when mixed with a second guest component. For example, we exhaustively investigate the Lennard-Jones interaction parameters of the second guest component and mix it with methane or xenon. The structure of the hydrate of the neat second guest species and the number of possible crystal structures by mixing are shown in Figures 4b and c. Since both xenon and methane are guest species forming type I structure, it is natural that two types of crystals appear when the second guest species prefers type II. Interestingly, three phases, I, II, and III, may appear by addition of a second guest species forming type I structure having a relatively strong interaction, even though both the two guest components are of species forming type I structure. To the best of our knowledge, no guest species with such interaction parameters have been found in practice, although some CFCs used as refrigerants may fall into this category. These molecules may also serve as phase change agents.

In this study, we employ a hypothetical bromine-like ideal gas Q instead of real bromine because bromine is liquid at room temperature and soluble in liquid water. To evaluate the phase-change ability of the gas-bromine mixture would require extra calculations to estimate the chemical potential of bromine dissolved in water, which is beyond the aim of this study. However, as shown in Figure 4(a), a low concentration of Q has the ability to alter the crystal structure of clathrate hydrate. Hence, even a very small amount of bromine dissolved in water is expected to act as a phase-change agent.

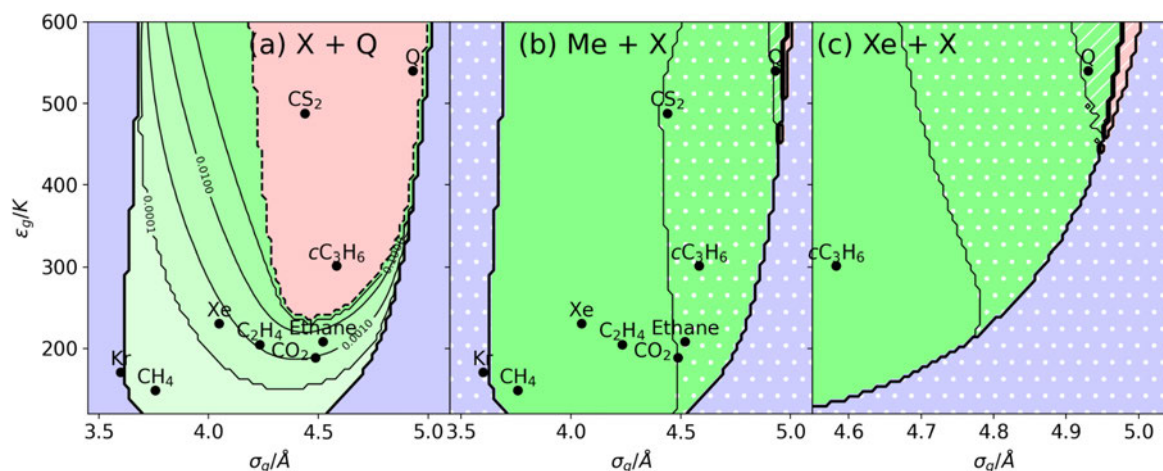


Figure 4. Phase diagrams of the binary gas hydrates plotted against the interaction parameters of one of the components, X. Total pressure of gases is 50 bar. The black dots represent the LJ interaction parameters of typical guest molecules shown in Table 1. (a) Contour diagram showing the phase-change ability of Q. The contours represent the minimum mole fraction of Q required to change its crystal structure to type II. The four thin solid contours correspond to the mole fractions of Q of 0.0001, 0.001, 0.01, and 0.1. The region where type II structure does not appear by mixing is filled in red. In the blue region, neat X forms type II structure by itself. (b) (c) Classifies the crystal structures appearing with respect to the interaction parameters of the guest component X. In (b) and (c) methane and xenon are the second components, respectively. The green, blue, and red fills indicate regions where the neat X forms type I, II, and III (CS-I, CS-II, and TS-I) crystal structures, respectively. The solid, dotted, and hatched fills indicate the appearance of one, two, and three phases by changing the mole fractions of the two components, respectively.

Conclusions

We discuss the features of the coexistence line on the GPD of the FK clathrate hydrate. It is shown that the coexistence line is linear and the slope and intercept are easily determined by the difference between the composition ratio and the host terms of the chemical potential of water molecules in the three canonical clathrate hydrate crystal structures, which are

irrelevant to guest species.

Based on these findings, we estimate the possible stable phases of the FK clathrates of group 14 elements. The small variety of crystal structures is due to the topological constraints imposed on the FK-type crystal structure, as in the case of FK clathrate hydrates. Moreover, we show that the use of a gas mixture can change the crystal structure of the clathrate hydrate (among the phases appearing on the GPD). An appropriate choice of the molecules enables us to form the type III structure by mixing gases, each of which forms type I structure in pure guest gas. Molecules that interact strongly with water, such as bromine, are expected to cause phase changes when they are mixed in small amounts and act as phase change agents. The same phenomenon must occur with group 14 clathrate compounds. From a practical point of view, the selection rule for the crystal structure of a group 14 clathrate compound, which is a semiconductor, deserves further investigation.

The GPD illustrates the most stable clathrate, if any, in the FK phases taking advantage of the fact that the diagram is rather insensitive to the temperature and the total pressure. It should be noted that the diagram does not tell us all the possible phases of the clathrate hydrates. More detailed investigations are required to deal with the non-FK phases that occur at high pressure, and with decomposition.

Acknowledgments

This work was supported by JSPS KAKENHI Grant Number 21H01047 and by Research Center for Computational Science in providing computational resource.

Appendix

The slope of the loci of state points on GPD

The loci of the state points for a guest species moves linearly by pressure on the GPD and its slope is almost common among any guest species. Here we derive the slope. The y coordinate of the state point is written using Eq. 3,

$$Y = \Delta\mu_c^{(\text{CS II})} - \Delta\mu_c^{(\text{HS I})}$$

$$= \sum_k \left(\alpha_k^{(\text{HS I})} - \alpha_k^{(\text{CS II})} \right) k_B T \ln \left(1 + \exp \left[\beta \left(\mu_g - f_g^{(k)} \right) \right] \right) \quad (\text{A1})$$

The chemical potential μ_g of an ideal gas can be written by summarizing the pressure-independent terms in B as

$$\exp \beta \mu_g = pB. \quad (\text{A2})$$

Then,

$$\begin{aligned} Y &= \sum_k \left(\alpha_k^{(\text{HS I})} - \alpha_k^{(\text{CS II})} \right) k_B T \ln \left(1 + \exp \beta \mu_g \exp \left(-\beta f_g^{(k)} \right) \right) \\ &= \sum_k \left(\alpha_k^{(\text{HS I})} - \alpha_k^{(\text{CS II})} \right) k_B T \ln \left(1 + pBF^{(k)} \right), \end{aligned} \quad (\text{A3})$$

where $F^{(k)} = \exp \left(-\beta f_g^{(k)} \right)$. Its derivative by pressure is

$$\frac{\partial Y}{\partial p} = \sum_k \left(\alpha_k^{(\text{HS I})} - \alpha_k^{(\text{CS II})} \right) k_B T \frac{BF^{(k)}}{pBF^{(k)} + 1}. \quad (\text{A4})$$

For simplicity, we assume $pBF^{(k)} \gg 1$ to erase “+1” in the denominator and obtain

$$\frac{\partial Y}{\partial p} \simeq \frac{\sum_k \left(\alpha_k^{(\text{HS I})} - \alpha_k^{(\text{CS II})} \right) k_B T}{p}. \quad (\text{A5})$$

We derive $\frac{\partial X}{\partial p}$ in the same way to obtain the slope:

$$\frac{dY}{dX} = \frac{\partial Y}{\partial p} \frac{\partial p}{\partial X} \simeq \frac{\sum_k \alpha_k^{(\text{HS I})} - \sum_k \alpha_k^{(\text{CS II})}}{\sum_k \alpha_k^{(\text{HS I})} - \sum_k \alpha_k^{(\text{CS I})}} = \frac{\frac{14}{80} - \frac{24}{136}}{\frac{14}{80} - \frac{8}{46}} = -\frac{23}{17}. \quad (\text{A6})$$

When the guest molecule is too large to be accommodated in the small cage, the contribution of small cages to Eq. A4 vanishes because $F^{(12)}$ is zero. However, the slope remains the same.

$$\frac{dY}{dX} \simeq \frac{\sum_{k \in \{14,15,16\}} \alpha_k^{(\text{HS I})} - \sum_{k \in \{14,15,16\}} \alpha_k^{(\text{CS II})}}{\sum_{k \in \{14,15,16\}} \alpha_k^{(\text{HS I})} - \sum_{k \in \{14,15,16\}} \alpha_k^{(\text{CS I})}} = \frac{\frac{8}{80} - \frac{8}{136}}{\frac{8}{80} - \frac{6}{46}} = -\frac{23}{17}. \quad (\text{A7})$$

Thus, the slope of the lines of state points is approximated by the numbers of the cages in the three canonical structures and is independent of the guest molecules or thermodynamic conditions.

Data Availability

The codes used to make figures are available in the GitHub repository:

<https://github.com/vitroid/vdwp>

References

- (1) Kvenvolden, K. A. Natural Gas Hydrate Occurrence and Issues. *Ann. N. Y. Acad. Sci.* **1994**, 715 (1 Natural Gas H), 232–246. <https://doi.org/10.1111/j.1749-6632.1994.tb38838.x>.
- (2) Glasby, G. P. Potential Impact on Climate of the Exploitation of Methane Hydrate Deposits Offshore. *Mar. Pet. Geol.* **2003**, 20 (2), 163–175. [https://doi.org/10.1016/S0264-8172\(03\)00021-7](https://doi.org/10.1016/S0264-8172(03)00021-7).
- (3) Ripmeester, J. A.; Ratcliffe, C. I.; Klug, D. D.; Tse, J. S. Molecular Perspectives on Structure and Dynamics in Clathrate Hydrates. *Ann. N. Y. Acad. Sci.* **1994**, 715 (1 Natural Gas H), 161–176. <https://doi.org/10.1111/j.1749-6632.1994.tb38832.x>.
- (4) Udachin, K. A.; Enright, G. D.; Ratcliffe, C. I.; Ripmeester, J. A. Structure, Stoichiometry, and Morphology of Bromine Hydrate. *Journal of the American Chemical Society*. 1997, pp 11481–11486. <https://doi.org/10.1021/ja971206b>.
- (5) Goldschleger, I. U.; Kerenskaya, G.; Janda, K. C.; Apkarian, V. A. Polymorphism in Br₂ Clathrate Hydrates. *J. Phys. Chem. A* **2008**, 112 (5), 787–789. <https://doi.org/10.1021/jp077562q>.
- (6) Stackelberg, M. v.; v. Stackelberg, M. Feste Gashydrate. *Naturwissenschaften*. 1949, pp 359–362. <https://doi.org/10.1007/bf00627172>.
- (7) Dutour Sikirić, M.; Delgado-Friedrichs, O.; Deza, M. Space Fullerenes: A Computer Search for New Frank--Kasper Structures. *Acta Crystallogr. A* **2010**, 66 (5), 602–615.

- (8) Bobev, S.; Sevov, S. C. Clathrates of Group 14 with Alkali Metals: An Exploration. *J. Solid State Chem.* **2000**, *153* (1), 92–105. <https://doi.org/10.1006/jssc.2000.8755>.
- (9) Bobev, S.; Sevov, S. C. Clathrate III of Group 14 Exists after All. *J. Am. Chem. Soc.* **2001**, *123* (14), 3389–3390. <https://doi.org/10.1021/ja010010f>.
- (10) Matsumoto, M.; Tanaka, H. On the Structure Selectivity of Clathrate Hydrates. *J. Phys. Chem. B* **2011**, *115* (25), 8257–8265. <https://doi.org/10.1021/jp203478z>.
- (11) Yarmolyuk, Y. P.; Kripyakevich, P. I. Mean Weighted Coordination Numbers and the Origin of Close-Packed Structures with Atoms of Unequal Size but Normal Coordination Polyhedra. *Sov. Phys. Crystallogr.* **1974**, *19*, 334–337.
- (12) Platteeuw, J. C.; van der Waals, J. H. Thermodynamic Properties of Gas Hydrates. *Mol. Phys.* **1958**, *1* (1), 91–96. <https://doi.org/10.1080/00268975800100111>.
- (13) Matsumoto, M.; Tanaka, H. Metastable Polymorphs of Clathrate Hydrate. *J. Phys. Soc. Jpn.* **2012**, *81* (Suppl.A), SA005. <https://doi.org/10.1143/JPSJS.81SA.SA005>.
- (14) Tanaka, H.; Nakatsuka, T.; Koga, K. On the Thermodynamic Stability of Clathrate Hydrates IV: Double Occupancy of Cages. *J. Chem. Phys.* **2004**, *121* (11), 5488–5493. <https://doi.org/10.1063/1.1782471>.
- (15) Tanaka, H.; Matsumoto, M. On the Thermodynamic Stability of Clathrate Hydrates V: Phase Behaviors Accommodating Large Guest Molecules with New Reference States. *J. Phys. Chem. B* **2011**, *115* (48), 14256–14262. <https://doi.org/10.1021/jp205067v>.
- (16) Tanaka, H.; Yagasaki, T.; Matsumoto, M. On the Thermodynamic Stability of Clathrate Hydrates VI: Complete Phase Diagram. *J. Phys. Chem. B* **2018**, *122* (1), 297–308. <https://doi.org/10.1021/acs.jpcc.7b10581>.
- (17) Tanaka, H.; Yagasaki, T.; Matsumoto, M. On the Occurrence of Clathrate Hydrates in Extreme Conditions: Dissociation Pressures and Occupancies at Cryogenic Temperatures with Application to Planetary Systems. *Planet. Sci. J* **2020**, *1* (3), 80. <https://doi.org/10.3847/PSJ/abc3c0>.
- (18) Frank, F. C.; Kasper, J. S. Complex Alloy Structures Regarded as Sphere Packings. II. Analysis and Classification of Representative Structures. *Acta Crystallographica*. 1959, pp 483–499. <https://doi.org/10.1107/s0365110x59001499>.
- (19) Matsumoto, M. Four-Body Cooperativity in Hydrophobic Association of Methane. *J. Phys. Chem. Lett.* **2010**, *1* (10), 1552–1556. <https://doi.org/10.1021/jz100340e>.
- (20) Vos, W. L.; Finger, L. W.; Hemley, R. J.; Mao, H. Novel H₂-H₂O Clathrates at High

- Pressures. *Phys. Rev. Lett.* **1993**, *71* (19), 3150–3153.
<https://doi.org/10.1103/PhysRevLett.71.3150>.
- (21) Londono, D.; Kuhs, W. F.; Finney, J. L. Enclathration of Helium in Ice II: The First Helium Hydrate. *Nature* **1988**, *332* (6160), 141–142. <https://doi.org/10.1038/332141a0>.
- (22) Efimchenko, V. S.; Kuzovnikov, M. A.; Fedotov, V. K.; Sakharov, M. K.; Simonov, S. V.; Tkacz, M. New Phase in the Water–hydrogen System. *J. Alloys Compd.* **2011**, *509*, S860–S863. <https://doi.org/10.1016/j.jallcom.2010.12.200>.
- (23) Fukuoka, H.; Iwai, K.; Yamanaka, S.; Abe, H.; Yoza, K.; Häming, L. Preparation and Structure of a New Germanium Clathrate, Ba₂₄Ge₁₀₀. *J. Solid State Chem.* **2000**, *151* (1), 117–121. <https://doi.org/10.1006/jssc.2000.8632>.
- (24) Madsen, G. K. H.; Schwarz, K.; Blaha, P.; Singh, D. J. Electronic Structure and Transport in Type-I and Type-VIII Clathrates Containing Strontium, Barium, and Europium. *Phys. Rev. B Condens. Matter* **2003**, *68* (12), 125212.
<https://doi.org/10.1103/PhysRevB.68.125212>.
- (25) Kirsanova, M. A.; Olenev, A. V.; Abakumov, A. M.; Bykov, M. A.; Shevelkov, A. V. Extension of the Clathrate Family: The Type X Clathrate Ge₇₉P₂₉S₁₈Te₆. *Angew. Chem. Int. Ed Engl.* **2011**, *50* (10), 2371–2374. <https://doi.org/10.1002/anie.201007483>.
- (26) Viennois, R.; Beaudhuin, M.; Koza, M. M. Strong Renormalization of Ba Vibrations in Thermoelectric Type-IX Clathrate Ba₂₄Ge₁₀₀. *Phys. Rev. B Condens. Matter* **2022**, *105* (5). <https://doi.org/10.1103/physrevb.105.054314>.
- (27) Fukuoka, H.; Ueno, K.; Yamanaka, S. High-Pressure Synthesis and Structure of a New Silicon Clathrate Ba₂₄Si₁₀₀. *J. Organomet. Chem.* **2000**, *611* (1), 543–546.
[https://doi.org/10.1016/S0022-328X\(00\)00404-6](https://doi.org/10.1016/S0022-328X(00)00404-6).
- (28) Karttunen, A. J.; Fässler, T. F.; Linnolahti, M.; Pakkanen, T. A. Structural Principles of Semiconducting Group 14 Clathrate Frameworks. *Inorg. Chem.* **2011**, *50* (5), 1733–1742. <https://doi.org/10.1021/ic102178d>.
- (29) Li, Z.; Hu, M.; Ma, M.; Gao, Y.; Xu, B.; He, J.; Yu, D.; Tian, Y.; Zhao, Z. Superhard Superstrong Carbon Clathrate. *Carbon N. Y.* **2016**, *105*, 151–155.
<https://doi.org/10.1016/j.carbon.2016.04.038>.
- (30) Martinez, A. D.; Krishna, L.; Baranowski, L. L.; Lusk, M. T.; Toberer, E. S.; Tamboli, A. C. Synthesis of Group IV Clathrates for Photovoltaics. *IEEE Journal of Photovoltaics* **2013**, *3* (4), 1305–1310.

- <https://doi.org/10.1109/JPHOTOV.2013.2276478>.
- (31) Belosludov, V. R.; Subbotin, O. S.; Krupskii, D. S.; Belosludov, R. V.; Kawazoe, Y.; Kudoh, J.-I. Physical and Chemical Properties of Gas Hydrates: Theoretical Aspects of Energy Storage Application. *Mater. Trans.* **2007**, *48* (4), 704–710.
<https://doi.org/10.2320/matertrans.48.704>.
- (32) Hester, K. C.; Sloan, E. D. sII Structural Transitions from Binary Mixtures of Simple sI Formers. *International Journal of Thermophysics*. 2005, pp 95–106.
<https://doi.org/10.1007/s10765-005-2355-1>.
- (33) Koyama, Y.; Tanaka, H.; Koga, K. On the Thermodynamic Stability and Structural Transition of Clathrate Hydrates. *J. Chem. Phys.* **2005**, *122* (7), 074503.
<https://doi.org/10.1063/1.1850904>.
- (34) Makino, T.; Tongu, M.; Sugahara, T.; Ohgaki, K. Hydrate Structural Transition Depending on the Composition of Methane Cyclopropane Mixed Gas Hydrate. *Fluid Phase Equilibria*. 2005, pp 129–133. <https://doi.org/10.1016/j.fluid.2005.04.011>.
- (35) Sugahara, T.; Makino, T.; Ohgaki, K. Isothermal Phase Equilibria for the Methane Ethylene Mixed Gas Hydrate System. *Fluid Phase Equilibria*. 2003, pp 117–126.
[https://doi.org/10.1016/s0378-3812\(02\)00313-8](https://doi.org/10.1016/s0378-3812(02)00313-8).
- (36) Abascal, J. L. F.; Sanz, E.; García Fernández, R.; Vega, C. A Potential Model for the Study of Ices and Amorphous Water: TIP4P/Ice. *J. Chem. Phys.* **2005**, *122* (23), 234511.
<https://doi.org/10.1063/1.1931662>.
- (37) Majid, Y. A.; Garg, S. K.; Davidson, D. W. Dielectric and Nuclear Magnetic Resonance Properties of a Clathrate Hydrate of Cyclopropane. *Can. J. Chem.* **1969**, *47* (24), 4697–4699. <https://doi.org/10.1139/v69-776>.
- (38) Kvamme, B.; Tanaka, H. Thermodynamic Stability of Hydrates for Ethane, Ethylene, and Carbon Dioxide. *J. Phys. Chem.* **1995**, *99* (18), 7114–7119.
<https://doi.org/10.1021/j100018a052>.
- (39) Hirschfelder, J. O.; Curtiss, C. F.; Bird, R. B. *Molecular Theory of Gases and Liquids. Physics Today*. 1955, pp 17–17. <https://doi.org/10.1063/1.3061949>.
- (40) Stephan, S.; Thol, M.; Vrabec, J.; Hasse, H. Thermophysical Properties of the Lennard-Jones Fluid: Database and Data Assessment. *J. Chem. Inf. Model.* **2019**, *59* (10), 4248–4265. <https://doi.org/10.1021/acs.jcim.9b00620>.
- (41) Matsumoto, M.; Yagasaki, T.; Tanaka, H. GenIce: Hydrogen-Disordered Ice

- Generator. *J. Comput. Chem.* **2018**, *39* (1), 61–64. <https://doi.org/10.1002/jcc.25077>.
- (42) Tanaka, H. Thermodynamic Stability and Negative Thermal Expansion of Hexagonal and Cubic Ices. *J. Chem. Phys.* **1998**, *108* (12), 4887–4893.
<https://doi.org/10.1063/1.475897>.
- (43) Guggenheim, E. A. *Mixtures: The Theory of the Equilibrium Properties of Some Simple Classes of Mixtures, Solutions and Alloys*; Clarendon Press, 1952.
- (44) Chakoumakos, B. C.; Rawn, C. J.; Rondinone, A. J.; Stern, L. A.; Circone, S.; Kirby, S. H.; Ishii, Y.; Jones, C. Y.; Toby, B. H. Temperature Dependence of Polyhedral Cage Volumes in Clathrate Hydrates. *Can. J. Phys.* **2003**, *81* (1-2), 183–189.
<https://doi.org/10.1139/p02-141>.
- (45) Takeya, S.; Hachikubo, A. Structure and Density Comparison of Noble Gas Hydrates Encapsulating Xenon, Krypton and Argon. *Chemphyschem* **2019**, *20* (19), 2518–2524.
<https://doi.org/10.1002/cphc.201900591>.
- (46) Takeya, S.; Hachikubo, A. Distortion of the Host Water Cages of Structure I Gas Hydrates: Structural Analysis of C₂H₄ Hydrate by Powder X-Ray Diffraction. *The Journal of Physical Chemistry C*. 2021, pp 28150–28156.
<https://doi.org/10.1021/acs.jpcc.1c09464>.
- (47) Adamova, T. P.; Subbotin, O. S.; Pomeransky, A. A.; Belosludov, V. R. Modeling of Phase Transition sI–sII in Binary Gas Hydrates of Methane and Ethane in Dependence on Composition of Gas Phase. *Comput. Mater. Sci.* **2010**, *49* (4), S317–S321.
<https://doi.org/10.1016/j.commatsci.2010.01.026>.
- (48) Zhdanov, R. K.; Adamova, T. P.; Subbotin, O. S. Modeling the Properties of Methane+ Ethane (Propane) Binary Hydrates, Depending on the Composition of Gas Phase State in Equilibrium with Hydrate. *Journal of Engineering* **2010**.
<https://doi.org/10.1134/S1810232810040041>.

TOC Graphics

